A shape manifold learning approach for indentation-based identification of material properties

Liang Meng, Piotr Breitkopf, Balaji Raghavan, Olivier Bartier, Xavier Hernot, Gérard Mauvoisin

CSMA 2015
12e Colloque National en Calcul des Structures
18-22 Mai 2015, Presqu'île de Giens (Var)

A shape manifold learning approach for indentation-based identification of material properties

L. Meng[1], P. Breitkopf[1], B. Raghavan[2], O. Bartier[2], X. Hernot[2], G. Mauvoisin[2]

[1] *Laboratoire Roberval, UMR 7337 UTC-CNRS, Université de Technologie de Compiegne, Compiegne, France, e-mail: liang.meng@utc.fr*
[2] *Laboratoire de Génie Civil et Génie Mécanique EA 3913, INSA de Rennes, 20 Avenue des Buttes de Coesmes, 35708 Rennes cedex, France*

Résumé — The conventional approach for the identification of the work hardening properties of a material by an indentation test usually relies on the force-displacement curve. However, finite element modeling of the indenter-specimen system is a complex task, and the unicity of the solution to the inverse problem of identifying material parameters using the force-displacement curve is not always guaranteed, especially for anisotropic materials. Also, the precise measurement of the displacement of the indenter tip is a complex task requiring the determination of the indenter frame compliance and indenter tip deformation. To alleviate all of these problems, we propose in this work an approach based solely on the 3D indentation imprint shape measured after indenter withdrawal, rather than relying on the minimization of the pointwise discrepancy between the experimental and simulated indentation curve. We first build a mathematical "shape space" of indentation shapes in which a lower-dimensional manifold of imprints admissible according to a postulated material constitutive law is approximated. Then, we solve the inverse problem by using a predictor-corrector algorithm minimizing the distance between the estimated solution and the experimental imprint in this shape space. Finally, we apply the proposed approach to an indentation test using a spherical tip indenter on a C100 steel specimen.
Mots clés — Identification ; Shape manifold learning ; Indentation test ; Reduced Order Modeling

1 Introduction

The identification of material work hardening properties by an indentation test [1, 2] is considered as non-destructive, especially when compared to the tensile test. With the help of indentation tests carried out on different scales, a wide range of materials can be characterized : metals, alloys, ceramic, concrete or even graded materials[3, 4, 5, 6] and the test can also be applied to an actual structure without the need for cutting-out a specimen for tensile testing.
The force applied to the indenter is recorded against the penetration depth over a sequence of time instants. This recorded indentation curve (P-h) curve is the primary information considered in the identification of material properties. A conventional deterministic identification approach is then applied to minimize the discrepancy between the simulated and measured P-h curves

$$J_h(\mathbf{c}) = \sum_{i=1}^{N_h} \left(\frac{h_i^s(\mathbf{c}) - h_i^e}{h_{max}^e} \right)^2, \tag{1}$$

where $\mathbf{c}$ is the vector of material parameters to be identified ; h_i is the corresponding penetration depth of indenter at the time instant $i = 1,2,3\cdots N_h$; the superscript 's' referring to simulation by the Finite Element Method (FEM), while 'e' represents 'experimental'. Mathematical programming procedures are then used to identify material properties by solving

$$\mathbf{c}^* = Argmin\Big(J_1(\mathbf{c})\Big). \tag{2}$$

However, coincident P-h curves [7, 8] may be obtained for different anisotropic materials and this can make the solution to the inverse problem non-unique. It is reasonable to assume that the residual deformation of the surface of the specimen after he indentation test would provide additional evidence since different materials are expected to show differing plastic piling-up or elastic sink-in effects. Extensive research has been devoted to combining the traditional indentation test with mapping the residual deformation (imprint) in order to provide more reliable information for the identification of material properties

[9, 10, 11]. In the problem of identification using the imprint shape i addition to the indentation curve, the cost function given by Eq.(1) may be augmented by :

$$J_u(\mathbf{c}) = \sum_{j=1}^{N_u} \left(\frac{u_j^s(\mathbf{c}) - u_j^e}{u_{max}^e} \right)^2, \tag{3}$$

where u_j is the vertical coordinate of point j measured against the initial surface of specimen ; N_u is the number of sample points chosen from the specimen surface, and this value depends on the resolution of the imprint scanning instrument and on the density of the FE mesh.
However, it has been shown that even a small noise in input data makes difficult the accurate identification of parameters[12]. Another factor of instability is the mesh dependency of the indentation curve and oscillations seen in the FE simulations[13]. Moreover, the two sources of errors given by $J_h(\mathbf{c})$ and $J_u(\mathbf{c})$ are impossible to compare numerically. [3] proposed to add weighting coefficients in front of each term, calibrated to make them comparable, however this approach is ad-hoc.
In the present work, we propose an original identification protocol based solely on the imprint shape. Following [15, 16], originally applied to the numerical assessment of spring-back for the deep drawing process, we build a shape space and apply the concept of shape manifold to describe all the imprint shapes admissible according to a postulated constitutive law. The shape manifold is constructed by a series of simulated shape imprints using Design of Experiments (DOE) and Proper Orthogonal Decomposition (POD). We then propose a family of manifold walking algorithms to determine the search direction. Finally, we apply the protocol to an indentation test using a spherical tip indenter on C100 steel.

2 Overall concept and formulation

We apply the method of Proper Orthogonal Decomposition (POD) to the collection of imprint shapes obtained by an indentation test. A typical finite element (FE) model and the residual deformation on the specimen are shown in Fig.1.

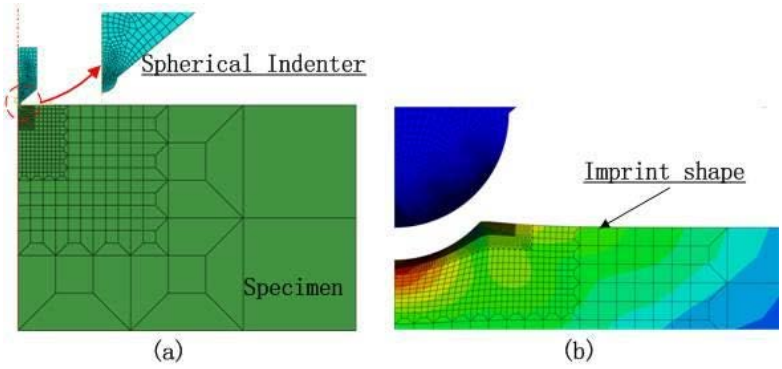

FIGURE 1 – FE simulation of indentation test and the residual displacement on the specimen

2.1 Construction of the shape space

We begin with M numerical experiments defined by an appropriate DOE for the varying set of design parameters $\mathbf{c}^{(i)}, i = 1,2\cdots M$. These design variables are the material parameters that need to be identified. The different imprint shapes $\mathbf{s}^{(i)} = \mathbf{s}(\mathbf{c}^{(i)})$ extracted from the simulation results are considered as imprint snapshots. The centered snapshot matrix $\mathbf{S}$ is calculated using the mean snapshot $\bar{\mathbf{s}}$

$$\mathbf{S} = [\mathbf{s}^{(1)} - \bar{\mathbf{s}}, \mathbf{s}^{(2)} - \bar{\mathbf{s}}, \cdots \mathbf{s}^{(M)} - \bar{\mathbf{s}}], \quad \bar{\mathbf{s}} = \frac{1}{M} \sum_{i=1}^{M} \mathbf{s}^{(i)}. \tag{4}$$

Singular value decomposition of $\mathbf{S}$ gives $\mathbf{S} = \mathbf{\Phi D V^T}$. The diagonal matrix $\mathbf{D}$ contains the singular values $d_i, i = 1,2\cdots M$; each column of $\mathbf{\Phi} = [\phi^{(1)}, \phi^{(2)} \cdots \phi^{(M)}]$ is an eigenvector of the covariance matrix $\mathbf{C} = \mathbf{S S^T}$ and is called a POD mode, and the corresponding eigenvalues are $\lambda_i = d_i^2$. Each snapshot $\mathbf{s}^{(i)}$

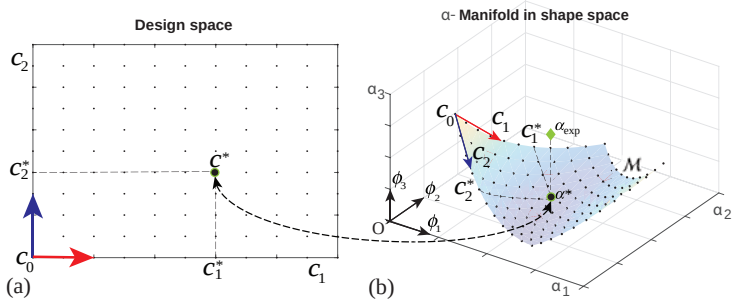

FIGURE 2 – Mapping between the design and α-space.

may then be accurately reconstructed

$$\mathbf{s}^{(i)} = \bar{\mathbf{s}} + \mathbf{\Phi}\boldsymbol{\alpha}^{(i)} = \bar{\mathbf{s}} + \sum_{j=1}^{M} \alpha_j^{(i)} \boldsymbol{\phi}^{(j)}, \tag{5}$$

where $\alpha_j^{(i)}$ is the projection coefficient for the i^{th} snapshot on the j^{th} mode

$$\alpha_j^{(i)} = \left(\boldsymbol{\phi}^{(j)}\right)^{\mathbf{T}} \left(\mathbf{s}^{(i)} - \bar{\mathbf{s}}\right), j = 1, 2 \cdots M. \tag{6}$$

The lower-dimensional approximation consists of using only the first $m \ll M$ (m is chosen according to an error threshold ε) most significant modes

$$\tilde{\mathbf{s}}_i = \bar{\mathbf{s}} + \sum_{j=1}^{m} \alpha_j^i \boldsymbol{\phi}_j; \varepsilon = 1 - \frac{\sum_{i=1}^{m} \lambda_i}{\sum_{j=1}^{M} \lambda_j}. \tag{7}$$

However, the difficulty in choosing m is to set an appropriate value for ε. In this work, rather than using Eq.(7), we exploit the concept of the α-manifold.

2.2 Manifold $\mathcal{M}$ of admissible shapes

For a set of M simulated imprint shapes, Eq.(6) gives their coordinates $\boldsymbol{\alpha}^1$, $\boldsymbol{\alpha}^2$ $\cdots$ $\boldsymbol{\alpha}^M$ in α-space. We make the fundamental assumption that all imprint shapes admissible according to a given material law lie on a smooth manifold

$$\mathcal{M}(\boldsymbol{\alpha}) = 0. \tag{8}$$

We use a parametric representation of $\mathcal{M}$

$$\alpha_i(\mathbf{c}) = \boldsymbol{p}^{\mathbf{T}}(\mathbf{c})\boldsymbol{a}^{(i)}, i = 1, 2 \cdots M, \tag{9}$$

with polynomial basis $\boldsymbol{p}$ and the coefficient vectors $\boldsymbol{a}^{(i)}$ approximated for all $\alpha_i^{(j)}, j = 1, 2 \cdots M$ by minimizing least-square error

$$\boldsymbol{a}^{(i)} = Argmin \frac{1}{2} \sum_{j=1}^{M} \left(\boldsymbol{p}^{\mathbf{T}}(\mathbf{c}^{(j)})\boldsymbol{a}^{(i)} - \alpha_i^{(j)}\right)^2. \tag{10}$$

For each point in the design space defined by the constitutive parameter values, we can find a corresponding point on the manifold by using Eq.(9). Also, each point on the manifold corresponds to an imprint snapshot and consequently to a set of parameter values in design space. Thus a one-to-one relationship is built up between the design space and the shape manifold in α-space (Fig.2). For the purpose of visualization, only a 3D section of this higher-dimensional space is presented.

2.3 Identification of material properties

The goal of the identification procedure is to minimize the distance between the simulated and experimental imprint ($\mathbf{s}_{exp}$) shapes in α-space. The projection of experimental imprint $\tilde{\mathbf{s}}_{exp}$ is

$$\tilde{\mathbf{s}}_{exp} = \bar{\mathbf{s}} + \mathbf{\Phi}\mathbf{\Phi}^{\mathbf{T}}(\mathbf{s}_{exp} - \bar{\mathbf{s}}) = \bar{\mathbf{s}} + \mathbf{\Phi}\boldsymbol{\alpha}_{exp}, \tag{11}$$

and it is represented by its coordinates $\boldsymbol{\alpha}_{exp}$ in "shape space". When comparing this with te experimental imprint, we note that the measurement noise is smoothed out by the POD modes. The projection to α-space may be thus considered as a *physics-based smoothing procedure*.
In the general case, the projection $\boldsymbol{\alpha}_{exp}$ will not lie on $\mathcal{M}$ due to the experimental noise (Fig.2). Our goal then is to find the closest point $\boldsymbol{\alpha}^*$ on $\mathcal{M}$ such that

$$\mathbf{c}^* = Argmin\|(\boldsymbol{\alpha}_{\text{exp}} - \boldsymbol{\alpha}(\mathbf{c}))\|, \alpha(\mathbf{c}) \in \mathcal{M}. \tag{12}$$

Therefore, the identification of material properties can be carried out in an at most M-dimensional space. We recall that $M \ll n$, where n is the dimensionality of the imprint shape vector $\boldsymbol{u}$ used in Eq.(3). The dimensionality of the search space may be further reduced to $m \ll M$ using Eq.(7). Taking into account Eq.(5) and (11), we note that the convergence criterion in Eq.(12) is equivalent to

$$\mathbf{s}^* = \mathbf{s}(\mathbf{c}^*) = \underset{\mathbf{s}}{\text{Argmin}}\|\tilde{\mathbf{s}}_{\text{exp}} - \mathbf{s}(\mathbf{c})\|. \tag{13}$$

2.4 Manifold walking algorithms

Extensive off-line simulations are needed to construct a global manifold that is suficiently accurate for identification purposes as it is always high-dimensional and nonlinear. In the present work, we propose an on-line approach that progressively constructs only the useful portion of $\mathcal{M}$ (local manifold) using the predictor-corrector strategy. The design space of each iteration step is usually called a design window, and the width and height of this window refer to the range of variation of the different parameters.

2.4.1 Panning

In this algorithm, the design window pans in the design space while the window size remains unchanged. For the first iteration step, we calculate a prediction with the initial design window. If the new prediction lies outside the window, we limit it to the window boundary and the next iteration window will be centered around this new prediction. We repeat this process until the prediction is located inside the current window and the convergence criterion in Eq.(12) is satisfied.

2.4.2 Zooming

In this algorithm, the first design of experiments covers the entire design space, after which the window size is halved with each successive iteration. In this algorithm, the new prediction always lies within the current window, and we center the new smaller design window around this new estimation value.

2.4.3 Panning & Zooming

The panning & zooming method combines both approaches. The idea of this algorithm is to use panning searching at the beginning until the estimation for the next iteration lies inside the current design window rather on the boundary, then we switch search schemes to zooming to improve the accuracy of the local manifold.

3 Numerical example

3.1 Problem description

The methodology is verified on an axisymmetric indentation test on C100 steel using a spherical tip indenter, the radius of which is 0.5 *mm*. The specimen was carefully sectioned and polished using fine emery papers (up to 1200 grit) and diamond suspensions (6 and 3 lm) to limit noise due to roughness. The simulation of the indenter test is carried out within ABAQUS using a FE model (Fig.1).

TABLE 1 – Iteration results using panning approach.

Iter	σ_y	n	$\Delta\sigma_y$	Δn	$\|\boldsymbol{\alpha}_{\text{exp}} - \boldsymbol{\alpha}^*\|$	ε_1	ε_2
1	205.0	0.225	30	0.05	0.0629	8.01%	8.78%
2	190.1	0.226	30	0.05	0.0327	4.15%	5.56%
3	175.1	0.239	30	0.05	0.0292	3.71%	5.16%
4	160.1	0.260	30	0.05	0.0219	2.79%	4.57%
5	145.1	0.275	30	0.05	0.0171	2.18%	4.20%
6	130.2	0.294	30	0.05	0.0118	1.50%	3.88%
7	115.4	0.312	30	0.05	0.0052	0.66%	3.58%
8	104.0	0.330	30	0.05	0.0030	0.38%	3.53%

Hollomon's power law is employed for the plastic properties [14] while the elastic portion is assumed to follow Hooke's law. The continuity at the elastic limit is enforced, resulting in

$$\sigma = \sigma_y \left(\frac{E}{\sigma_y} \right)^n \varepsilon^n, \tag{14}$$

where σ is the equivalent stress, ε refers to the total strain. The behavior law of material is thus described by three parameters : yield stress σ_y, strain hardening exponent n and Young's modulus E. E is fixed at 21000MPa, while σ_y and n will be identified. The parameters are identified in a rather large design space ($n \in [0.1, 0.5]$, $\sigma_y \in [50, 400]$) in order to verify the robustness of the methodology. The error in identification by comparing the imprint shapes is calculated by

$$\varepsilon_1 = \frac{\|\tilde{\mathbf{s}}_{\text{exp}} - \mathbf{s}(\sigma_y, n)\|}{\|\tilde{\mathbf{s}}_{\text{exp}}\|}. \tag{15}$$

In order to demonstrate the advantage of using this adaptive mathematical shape manifold, we also compute the error between the imprint shape derived by identified parameters and real experimental data

$$\varepsilon_2 = \frac{\|\mathbf{s}_{exp} - \mathbf{s}(\sigma_y, n)\|}{\|\mathbf{s}_{\text{exp}}\|} \tag{16}$$

3.2 Results and discussion

3.2.1 panning

The iteration history of identification using the panning algorithm is shown in Table.1. The designs of experiments are centered around successive sets of σ_y and n. $\Delta\sigma_y$ and Δn are the size of design space. ε_1 and ε_2 are identification errors of each iteration, namely the error between the simulated imprint shape computed by σ_y and n and real experimental imprint (Eq.(15)) or its projection in shape space (Eq.(16)).

Successive design spaces and corresponding local manifolds are shown in Fig.3-5. The green diamond, referring to the projection of experiment imprint in α-space, converges to the center of the local coordinate system, which also implies that the estimated imprint converges to $\mathbf{s}_{exp}$. The black dot in the design space represents the current estimation parameters corresponding to the point on $\mathcal{M}$ closest

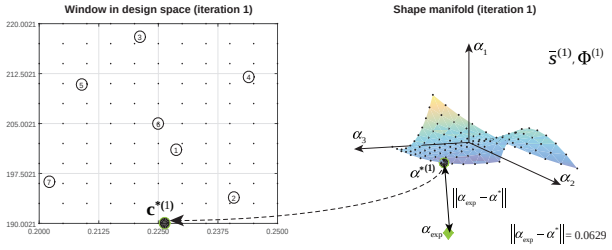

FIGURE 3 – Identification in design space and corresponding local manifold (step 1).

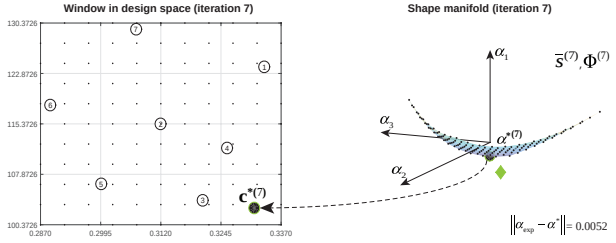

FIGURE 4 – Identification in design space and corresponding local manifold (step 7).

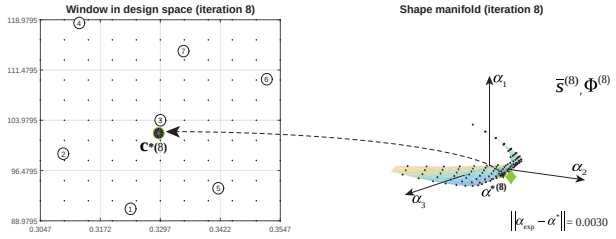

FIGURE 5 – Identification in design space and corresponding local manifold (step 8).

to the projection of experimental imprint. The local manifolds in this panning method are not accurate estimations simply because we are only using a quadric surface to approximate $\mathcal{M}$ in a relatively wide range($\Delta\sigma_y = 30, \Delta n = 0.05$). With the panning method, we can only obtain a general estimation for the material parameters. The accuracy may be improved either by increasing the degree of polynomial basis or by shrinking the size of window.

3.2.2 zooming

For this algorithm,the convergence of the material properties is shown in Table.2, where σ_y stabilized around 105 and n around 0.326. Clearly, the error ε_2 stabilized at 3.6% after only 3 iteration steps, while the error ε_1 drops to around 1% using the projected imprint in shape space. Even though the error ε_1 in the 4^{th} iteration is smaller than the last one, we still prefer the material identified in the last step for the reason that the local manifold is more accurate so as to obtain the projection of the experimental imprint. The last manifold is considered accurate since the identification is carried out in a small window size and the material parameters vary only in a small range : 2.5 for σ_y and 0.002 for n. Several steps of imprint snapshots and the experimental imprint are compared (Fig.6). It is clear that the simulated imprint shapes will concentrate around the experimental one when the local manifold patch size decreases.

3.2.3 panning & zooming

Finally, a combined algorithm of panning and zooming is applied. A similar estimation of material properties is obtained(Table.3). In the first four steps, the panning method is introduced to iteratively locate the most promising zone, and during these steps the design window remains the same size. Next,

TABLE 2 – Iteration results using regular zooming approach.

Iter	σ_y	n	$\Delta\sigma_y$	Δn	$\|\boldsymbol{\alpha}_{\text{exp}} - \boldsymbol{\alpha}^*\|$	ε_1	ε_2
1	250.0	0.250	320	0.3	0.2512	31.97%	32.16%
2	99.79	0.394	160	0.15	0.0155	1.97%	4.25%
3	98.32	0.336	80	0.08	0.0150	1.90%	3.89%
4	98.65	0.331	40	0.04	0.0056	0.71%	3.59%
5	112.44	0.327	20	0.02	0.0147	1.87%	3.57%
6	105.80	0.326	10	0.01	0.0092	1.16%	3.54%
7	105.46	0.326	5	0.005	0.0079	1.01%	3.57%
8	105.79	0.326	2.5	0.002	0.0069	0.87%	3.57%

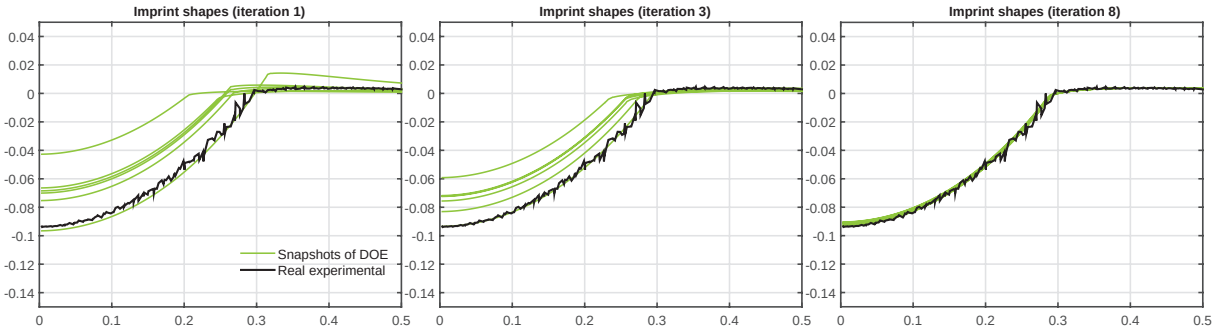

FIGURE 6 – Experimental imprint and numerical snapshots (zooming algorithm).

the zooming algorithm is adopted in order to improve the accuracy of the local manifold for better identification. The first searching algorithm is automatically switched with the second one as soon as the estimate for the next iteration is located inside the current design space rather than on the boundary.

TABLE 3 – Iteration results using panning & zooming.

Iter	σ_y	n	$\Delta\sigma_y$	Δn	$\|\alpha_{\text{exp}} - \alpha^*\|$	ε_1	ε_2
1	175.0	0.300	40	0.04	0.1989	25.31%	25.56%
2	155.0	0.280	40	0.04	0.0697	8.87%	9.62%
3	135.2	0.287	40	0.04	0.0175	2.22%	3.98 %
4	120.5	0.307	40	0.04	0.0083	1.05%	3.68%
5	107.0	0.326	20	0.02	0.0059	0.75%	3.54%
6	108.0	0.323	10	0.01	0.0121	1.53%	3.57%
7	106.7	0.323	5	0.005	0.0089	1.13%	3.56%
8	107.0	0.324	2.5	0.002	0.0096	1.22%	3.57%

It may be concluded from the iteration histories of all the convergence algorithms that the combined zooming & panning approach better convergence of *both* parameters. In addition, the robustness of the identification procedure in lower-dimensional $\alpha-$space is confirmed by using different initial points for the three algorithms which lead to identical material parameters. The different searching patterns are shown in Fig.7.

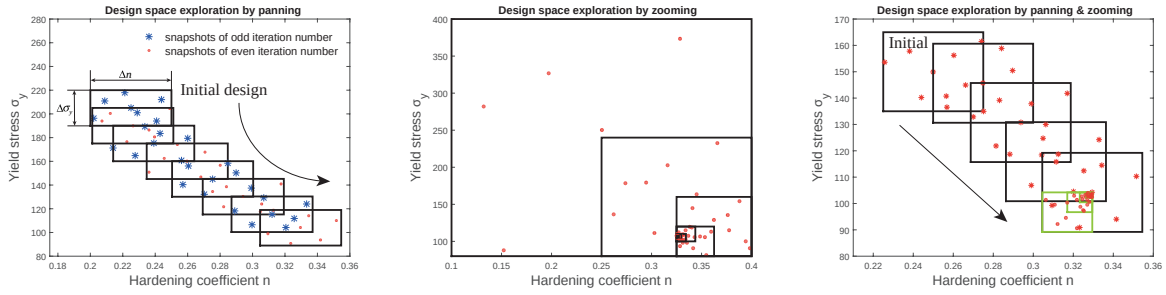

(a) Panning (b) Zooming (c) Panning & Zooming

FIGURE 7 – Searching patterns of different algorithms.

4 Conclusion and perspectives

In this paper, the authors have proposed a complete protocol for the identification of material work hardening properties, using only the imprint shape of an instrumented indentation test. By adopting the concept of the shape manifold, satisfactory results were obtained using a variety of algorithms. Almost

identical power law work hardening parameter sets (σ_y, n) are obtained with different convergence algorithms even when starting from very different initial points. The error between the experimental imprint and simulated imprint with identified parameters can be controlled to a considerably low level, around 1%.
That being said, our protocol can and should be improved in order to reuse the imprints in the current iteration if they are also situated in the design space of next iteration, as this will yield a significant reduction in computation time.

Acknowledgements

This work was carried out in the framework of the Labex MS2T, which was funded by the French Government, through the program " Investments for the future " managed by the National Agency for Research (Reference ANR-11-IDEX-0004-02). This work is also funded by the China Scholarship Council (CSC).

Références

[1] B.W.Mott. *Micro-indentation hardness testing*, Butterworths Scientific Publications,1956.

[2] D.Tabor. *The hardness of metals*, Vol.10, ClarendonP, 1951.

[3] C. K. Moy, M. Bocciarelli, S. P. Ringer, G. Ranzi. *Identification of the material properties of al 2024 alloy by means of inverse analysis and indentation tests*, Materials Science and Engineering : A 529 (2011) 119-130.

[4] R. C. Paietta, S. E. Campbell, V. L. Ferguson. *Influences of spherical tip radius, contact depth, and contact area on nanoindentation properties of bone*, Journal of biomechanics 44 (2) (2011) 285-290.

[5] [5] R. F. Gibson. *A review of recent research on nanoindentation of polymer composites and their constituents*, Composites Science and Technology 105 (2014) 51-65.

[6] C. Moussa, X. Hernot, O. Bartier, G. Delattre, G. Mauvoisin. *Identification of the hardening law of materials with spherical indentation using the average representative strain for several penetration depths*, Materials Science and Engineering : A 606 (2014) 409-416.

[7] X. Chen, J. J. Vlassak. *Numerical study on the measurement of thin film mechanical properties by means of nanoindentation*, Journal of Materials Research 16 (10) (2001) 2974-2982.

[8] J. Alkorta, J. Martinez-Esnaola, J. G. Sevillano. *Absence of one-to-one correspondence between elastoplastic properties and sharp-indentation load ?penetration data*, Journal of materials research 20 (02) (2005) 432-437.

[9] K. Zeng, E. Soderlund, A. Giannakopoulos. D. Rowcliffe. *Controlled indentation : a general approach to determine mechanical properties of brittle materials*, Acta Materialia 44 (3) (1996) 1127-1141.

[10] B. Taljat, T. Zacharia, F. Kosel. *New analytical procedure to determine stress-strain curve from spherical indentation data*, International Journal of Solids and Structures 35 (33) (1998) 4411-4426.

[11] K. Matsuda. *Prediction of stress-strain curves of elastic-plastic materials based on the vickers indentation*, Philosophical Magazine A 82 (10) (2002) 1941-1951.

[12] T. Capehart, Y. Cheng. *Determining constitutive models from conical indentation : Sensitivity analysis*, Journal of materials research 18 (04) (2003) 827-832.

[13] Y. Liu, B. Wang, M. Yoshino, S. Roy, H. Lu, R. Komanduri. *Combined numerical simulation and nanoindentation for determining mechanical properties of single crystal copper at mesoscale*, Journal of the Mechanics and Physics of Solids 53 (12) (2005) 2718-2741.

[14] J. Marteau, S. Bouvier, M. Bigerelle. *Review on Numerical Modeling of Instrumented Indentation Tests for Elastoplastic Material Behavior Identification*, Archives of Computational Methods in Engineering, 2014, pp : 1-17.

[15] B. Raghavan, G. Le Quilliec, P.Breitkopf et. al. *Numerical assessment of springback for the deep drawing process by level set interpolation using shape manifolds*, International Journal of Material Forming, December 2014, Volume 7, Issue 4, pp 487-501.

[16] B. Raghavan, P.Breitkopf et. al. *Towards a space reduction approach for structural shape optimization*, Structural & Multidisciplinary Optimization, 2013, Volume 48, Issue 5, pp 987-1000.